Experimental Determination of the Helium-Metal Interaction Potential by Interferometry of Nanostructured Surfaces

C. Huang,* D. A. MacLaren, J. Ellis, and W. Allison

Cavendish Laboratory, University of Cambridge, J. J. Thomson Avenue, Cambridge, CB3 0HE, United Kingdom

(Received 16 December 2005; published 28 March 2006)

We present a direct experimental comparison of the helium-surface interaction potential for two unreconstructed metal surfaces. We analyze phase shifts in helium atom scattering from a nanostructured bimetallic surface to yield the relative shape and position of an adsorbate's potential with respect to the reference defined by the substrate. In our prototype system, submonolayer growth of Ni on Cu(100), the He-Ni/Cu(100) potential has an attractive well that is 1.6 ± 0.4 meV shallower, and a repulsive wall 0.11 ± 0.03 Å closer to the ion cores, compared to the He-Cu(100) potential. Our observations provide a ready test of state-of-the-art theoretical calculations.

DOI: 10.1103/PhysRevLett.96.126102 PACS numbers: 68.49.Bc, 34.50.−s, 39.20.+q

Weak interatomic interactions, such as van der Waals and dispersive forces, underpin processes as diverse as physisorption [1–3] and protein folding. Their study is of current interest because these forces also govern the implementation of nanotechnology and surface interactions on atom chips [4]. However, precise studies of weak interactions are difficult, both theoretically and experimentally. The scattering of a rare gas atom from a low-index metal surface is an ideal prototype because it is amenable to both experiment and calculation. Theoretical helium-metal potentials are now available [2,3] but a difficulty arises experimentally because low-index, metallic surfaces appear flat and almost mirrorlike to thermal energy helium atoms. The absence of lateral corrugation means that diffraction [5] and selective adsorption processes [6] are extremely weak and therefore cannot be used to derive the helium-metal interaction potential. As a consequence, much of recent discussion has focused on experimentally accessible but indirect parameters such as "anticorrugation" [2,5,7], rather than the absolute position of the repulsive wall, or the depth of the attractive well. Both the well and wall of the potential contribute to the phase of the scattered wave; but these contributions cannot be determined directly since the experiment is insensitive to the absolute phase. In the present Letter we address the problem by using a heterogeneous, two-component surface in which one component provides a phase reference against which the relative scattering phase of the second component can be measured. In particular, we show that the technique extracts both the relative position of the repulsive wall and the depth of the attractive well with high precision.

We begin by outlining our methodology. In essence, our experiment is atom interferometry, since it combines the signal scattered from a sample and a reference. In practice, we study a submonolayer heteroepitaxial thin-film system, where the substrate provides the "reference" potential while the overlayer defines the "sample." For a typical experiment and in the absence of strong corrugation, helium scattering is well described by the JWKB approximation. Helium atoms scattered from adjacent atomic terraces, (A) and (B) of Fig. 1(a), in a thin-film system have a relative phase difference given by

$$\phi_{AB} = 2k_i\left\{\int_{z_t^B}^{\infty}\sqrt{\cos^2\theta_i - \frac{V_B(z)}{E_0}}dz - \int_{z_t^A}^{\infty}\sqrt{\cos^2\theta_i - \frac{V_A(z)}{E_0}}dz\right\}, \quad (1)$$

where $V_{A/B}(z)$ is the laterally averaged interaction potential between helium atoms and the A/B surface as a function of surface normal distance, z. The classical turning point above the A/B surface, $z_t^{A/B}$, is a function of incident angle θ_i and kinetic energy, $E_0 = \hbar^2 k_i^2/2m_{He}$. The origin of z is chosen at the substrate's outermost nuclear plane. In a scattering experiment, the observed intensity varies with

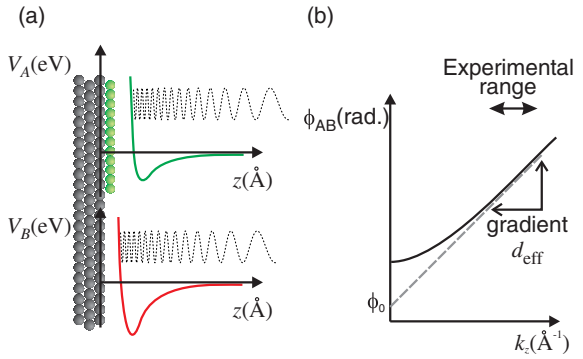

FIG. 1 (color online). (a) Schematic He interferometry of a submonolayer, two-dimensional overlayer (A) on a reference substrate (B), with different He-surface potentials V_A and V_B, respectively. The phase of impinging He atoms is modulated by the surface potential well. (b) The resultant variation in the phase difference ϕ_{AB} plotted as a function of the perpendicular wave vector, k_z. The variation has a complicated functional form at small k_z but is approximately linear within a typical experimental range, with best-fit intercept ϕ_0 and gradient d_{eff}.

$\cos\phi_{AB}$, giving rise to interference fringes, as will be shown. It is sometimes overlooked that the well has a substantial influence on the measured signal. Helium matter waves "refract" under its influence, giving rise to an additional phase contribution that affects *all* observable data. The resulting phase difference ϕ_{AB} is sketched as a function of the perpendicular wave vector $k_z = 2k_i \cos\theta_i$ in Fig. 1(b). A full knowledge of the phase difference would allow the differences between $V_A(z)$ and $V_B(z)$ to be determined *exactly*. In practice, however, a typical experiment is limited to a small range of k_z over which ϕ_{AB} will vary approximately linearly with k_z. Thus, the observed dependence can be written

$$\phi_{AB}(k_z) = k_z d_{\text{eff}} + \phi_0, \tag{2}$$

where the parameters d_{eff} and ϕ_0 will depend upon the range of k_z sampled. All of the structural parameters are contained in Eq. (2). The observed intensity is then modulated by nonstructural parameters, which describe Debye-Waller scattering and variations in the instrumental response. A general form for the observed intensity is

$$I(k_z) = P_1(k_z)\cos[\phi_{AB}(k_z)] + P_2(k_z), \tag{3}$$

where P_1 and P_2 are slowly varying functions of k_z to describe an envelope and which we represent by second order polynomials [8]. In practice, we determine d_{eff} from the usual, transform-based analysis of such lattice-rod scans [8,9]. The other structural parameter, ϕ_0, is determined from a fit to the measurements, using Eq. (3).

In general, when $V_A(z) \neq V_B(z)$, the phase offset ϕ_0 is finite and d_{eff} will differ from the ion-core separation between terraces A and B, d_{AB}. Differences between d_{eff} and d_{AB} have been observed previously in the Ag/Ag(100) [10], Fe/Ag(100) [11], and CO/Cu(100) [12] systems. In the first two cases, the effect was primarily geometric; the overlayer forms small islands (<6 atoms diameter), whose size leads either to a smoothing of the electron density (Smoluchowski effect) [10] or an increase in the van der Waals interaction at positions between islands [11]. The latter effect was modeled by the addition of a simple square well to the potential. In a study of the CO/Cu(100) system, on the other hand, a lattice-rod scan was modeled by shifting the substrate potential outwards while maintaining its form. In each case, the data gave a phenomenological description of the potential, being used *either* to discuss variations to its absolute position *or* to suggest alterations to the potential well. As we will now show, a full analysis of the specular lattice-rod scan can be used to extract quantitative data on both the potential's position *and* form.

Our prototype system is the submonolayer epitaxial growth of nickel on copper(100) ["Ni/Cu(100)"], chosen because (i) Ni and Cu have a small lattice mismatch (<3%), driving pseudomorphic growth and the formation of well-ordered, two-dimensional Ni islands at 280 K [13,14], (ii) Ni and Cu surfaces have significantly different electronic structures, being dominated by $3d$ and sp bands at the Fermi level, respectively [15], and (iii) several He-Cu(100) potentials have been calculated, ensuring a well-defined phase reference. In addition, the unreconstructed Ni overlayer is precisely the type of system for which an empirical determination of the He-metal potential would not have been previously possible.

The experiments were conducted on the Cambridge helium atom diffractometer, which is described elsewhere [16] and had a base pressure of 2×10^{-10} mbar. A nominally flat Cu(100) substrate (Surface Preparation Laboratory, The Netherlands) was cleaned by repeated cycles of Ar^+ sputtering (30 min, 800 eV, 5 μA/cm^2 at 300 K) and annealing (30 min at 800 K), until only a narrow, intense specular ^{4}He reflection was observed. Nickel deposition was performed using a water-cooled electron-bombardment evaporator which typically increased the chamber pressure by less than 1×10^{-10} mbar. Strong oscillations in the helium specular intensity during deposition at 280 K confirmed a two-dimensional, layer-by-layer growth mode for the first few monolayers and allowed the deposition rate to be calibrated as $\sim 1 \times 10^{-3}$ ML/s. Deposition of 0.5 ML Ni was conducted at 280 K, a temperature chosen to ensure well-ordered, pseudomorphic growth [13], but to preclude alloying [13,17]. A spot-profile analysis [13] indicates the formation of square, two-dimensional Ni islands with an average dimension of 56 Å, large enough that small-island effects [10,11] can be neglected.

Our main experimental results are presented in Fig. 2, which shows two lattice-rod scans, taken from (a) a randomly stepped Cu(100) surface (prepared by a mild sputtering—60 s, 800 eV, 4 μA at 240 K) and (b) the 0.5 ML Ni/Cu(100) surface described above. The data were taken by measuring the specular intensity as a function of incident angle θ_i with a fixed beam energy ($k_i = 11.16$ Å^{-1}). Clear oscillations are observed, arising from Bragg interference between atoms scattered from the reference [Cu(100) substrate] and sample (Ni overlayer), respectively. A Fourier analysis [8,9] of Fig. 2(a) confirmed the calibration of the helium beam energy and the scattering geometry with respect to the known bulk Cu(100) lattice spacing of 1.81 Å. For the chemically homogeneous Cu(100) surface the term ϕ_0 should be zero, as confirmed by the close agreement in position of the maxima and their expected positions, indicated by vertical dashed lines.

A Fourier transform of Fig. 2(b) also yielded a single significant peak, indicating that the vertical morphology was dominated by monatomic Ni-Cu steps and that double-layer features can be ignored [9]. A visual comparison of the two curves in Fig. 2 shows that there is a significant difference in the period of the oscillations that cannot be explained by the small difference in internuclear separations. The dashed vertical lines in Fig. 2(b) indicate the expected positions of maxima from an outward shift in the substrate potential by the Ni-Cu internuclear spacing, d_{AB},

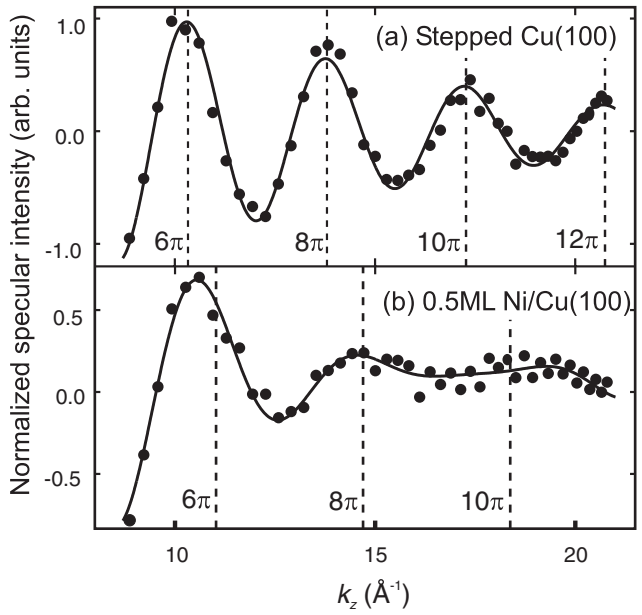

FIG. 2. Specular lattice-rod scans for helium atoms scattered from (a) a randomly stepped Cu(100) surface prepared by mild sputtering and (b) 0.5 ML Ni/Cu(100) grown at 280 K. The data are shown after subtraction of the $P_2(k_z)$ term of Eq. (3) and the smooth curves are fits to Eqs. (3) and (2). (Oscillation amplitudes are typically ~30% of the scattered intensity [8].) Dashed vertical lines indicate the positions of intensity maxima expected from the known ion-core spacings.

which is known to be 1.71 ± 0.01 Å from LEED measurements and *ab initio* theory [18–20]. Neither the position nor the spacing of the maxima are correct. We conclude that the differences between the lattice-rod scans arise primarily from the different atom-surface potentials experienced at Cu-exposed and Ni-exposed surface regions.

Analysis of the data, using Eq. (3), encodes the differences in potential into two experimental parameters $d_{\text{eff}} = 1.52$ Å and $\phi_0 = 2.61$ rad. In order to relate these parameters to quantitative differences in atom-surface potential, we first define a reference potential [16] V_B. We will present results for three distinct potentials but the analysis is largely independent of our choice. The overlayer potential V_A is then generated from the reference potential by means of a two-parameter transformation, $V_A(z) \leftarrow \alpha V_B(z - \beta)$, where α gives a linear scaling in energy and β translates the z scale. Many transformations are possible and the optimal choice may differ if, for example, the softness of the potential was to be extracted rather than the well depth, or if more fitted parameters were desired. Here, our choice is driven by: (i) the wish to have the same number of experimental observables (d_{eff} and ϕ_0) as fitting parameters, (ii) the ability to vary the well depth and the position of the wall independently, and (iii) our observation that α and β allow a unique solution to be determined. In practice, we have tried several different transforms satisfying the above two requirements and find the fitted results to be largely independent.

To illustrate the method, Fig. 3 shows two overlaid contour plots of d_{eff} and ϕ_0, calculated as a function of transformation vectors α and β and plotted as full and dotted lines, respectively. The contours are calculated using the potential of Ref. [16] as a reference, then applying Eq. (1) to it and the transformed potentials, separated in z by the known internuclear separation of $d_{AB} = 1.71 \pm 0.01$ Å. A unique fit to the data is found readily and is shown as a vertical cross in Fig. 3. The He-overlayer potential is constructed by applying the transformation. Figure 4 compares the reference Cu(100) potential and the experimental He-Ni/Cu(100) potential. For clarity, the curves are shifted in z such that the ion cores coincide. Figure 4 demonstrates that both the potential well and the repulsive wall of the He-Ni overlayer potential differ from those of the reference. In particular, the attractive well is 1.4 ± 0.4 meV shallower and the turning point at 50 meV is shifted inwards by 0.11 ± 0.04 Å.

We find the above relative results to be robust and largely independent of the forms of reference potential and parameterization. The method is precise enough to describe the relative shape and position of the modified potential with respect to the reference. As demonstration, Table I compares the above results (first row) with those determined using either a different form of potential or a different transformation from reference to overlayer potentials. The three He-Cu potentials chosen are calculated elsewhere by (i) a smoothed pairwise summation calculation [16], (ii) an *ab initio* self-consistent field (SCF) method [21], and (iii) combining a repulsive Hartree-Fock energy and a damped van der Waals attraction [22,23]. Each potential is used with the α, β transformation described above and also (in brackets) by alternative transformation, which expands the energy scale of the

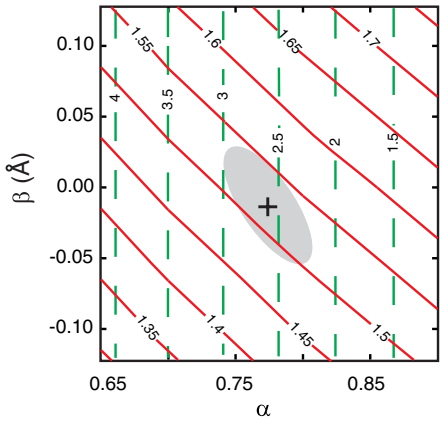

FIG. 3 (color online). A contour plot of simulated variations in d_{eff} (solid curves, in Å) and in ϕ_0 (dashed curves, in radians) depending on the transformation parameters α and β as defined in the text and using the first potential of Table I. The experimental result is indicated by the vertical cross, giving $d_{\text{eff}} = 1.52$ Å and $\phi_0 = 2.61$ rad. The shaded area gives the experimental uncertainty. Values of transformation parameters deduced from the plot are $\alpha = 0.77$ and $\beta = -0.01$ Å.

TABLE I. Calculated parameters for the empirical He-Ni/Cu(100) potential using different reference potentials. Positive ΔD represent a shallower well and positive turning-point values indicate an inward shift of the turning point at 50 meV with respect to the reference. Results from the second parameterization (see text) are in parentheses.

Reference	ΔD (meV)	Δz (Å)
[16]	1.4 ± 0.4	0.11 ± 0.03
[21]	1.6 ± 0.4 (2.0 ± 0.5)	0.11 ± 0.04 (0.10 ± 0.03)
[22,23]	1.5 ± 0.4 (1.5 ± 0.4)	0.11 ± 0.03 (0.11 ± 0.03)

attractive contribution while keeping the repulsive contribution the same. The two transformations operate differently on the well and wall of the potential. Specifically, an increase in well depth moves the wall outwards in the first transformation and inwards with the second. Irrespective of the transformation, or the reference potential, the same quantitative features emerge from the analysis (Table I). We conclude that our approach is robust and that the measurements indicate a He-Ni/Cu(100) potential with a shallower well and a closer wall. The properties of a Ni overlayer may differ from those of a Ni(100) surface, but we attribute most of the observed differences to the electronic configurations of Cu and Ni. Compared to Cu (ground electronic state: $[\mathrm{Ar}]3d^{10}4s^{1}$), the Ni overlayer (ground electronic state: $[\mathrm{Ar}]3d^{8}4s^{2}$) appears (i) to be less polarizable, since the attractive well is shallower and (ii) to have enhanced short-range attractive forces, since the repulsive wall is retracted. The observation of weaker long-range forces is in accord with previous calculations, based on He atom polarization and substrate dielectric function [24]; however, at a quantitative level, differences

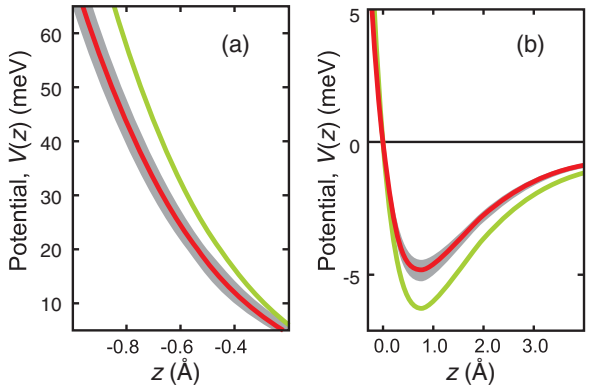

FIG. 4 (color online). The empirical He-Ni/Cu(100) potential and its experimental uncertainty (solid line with shading) compared directly to the He-Cu(100) reference potential (solid line) [16], both as a function of surface normal distance z from their respective ion cores. The z axis is chosen to have its origin at the zero crossing of the He-Cu(100) potential. (a) The region of the repulsive wall, and (b) the region of the attractive well.

in C_3 and C_5 coefficients for Cu and Ni only account for a fraction of the observed effect. The measured shift in the replusive wall contrasts with expectation of a previous Hartree-Fock, SCF calculation [21], which indicated an arrangement of turning points for Cu(100) and Ni(100) that is the reverse of our observations. A state-of-the-art density-functional theory calculation is still lacking on the Ni/Cu(100) surface but is clearly now warranted.

*Electronic address: ch309@cam.ac.uk

[1] R. D. Diehl, T. Seyller, M. Caragiu, G. S. Leatherman, N. Ferralis, K. Pussi, P. Kaukasoina, and M. Lindroos, J. Phys. Condens. Matter **16**, S2839 (2004).
[2] N. Jean, M. I. Trioni, G. P. Brivio, and V. Bortolani, Phys. Rev. Lett. **92**, 013201 (2004).
[3] M. Petersen, S. Wilke, P. Ruggerone, B. Kohler, and M. Scheffler, Phys. Rev. Lett. **76**, 995 (1996).
[4] J. D. Perreault and A. D. Cronin, Phys. Rev. Lett. **95**, 133201 (2005).
[5] K. H. Rieder, G. Parschau, and B. Burg, Phys. Rev. Lett. **71**, 1059 (1993).
[6] P. Cortona, M. G. Dondi, and F. Tommasini, Surf. Sci. **261**, L35 (1992).
[7] J. F. Annett and R. Haydock, Phys. Rev. Lett. **53**, 838 (1984).
[8] P. C. Dastoor and W. Allison, Surf. Sci. **433–435**, 99 (1999).
[9] D. Green, D. A. MacLaren, W. Allison, and P. C. Dastoor, J. Phys. D: Appl. Phys. **35**, 3216 (2002).
[10] P. Bedrossian, B. Poelsema, G. Rosenfeld, L. C. Jorritsma, N. N. Lipkin, and G. Comsa, Surf. Sci. **334**, 1 (1995).
[11] S. Terreni, P. Cantini, M. Canepa, and L. Mattera, Phys. Rev. B **56**, 6490 (1997).
[12] J. Ellis, K. Hermann, F. Hofmann, and J. P. Toennies, Phys. Rev. Lett. **75**, 886 (1995).
[13] C. Huang, D. A. Maclaren, and W. Allison, J. Phys.: Conf. Ser. **19**, 182 (2005).
[14] J. Shen, J. Giergiel, and J. Kirschner, Phys. Rev. B **52**, 8454 (1995).
[15] M. Hochstrasser, N. Gilman, R. F. Willis, F. O. Schumann, J. G. Tobin, and E. Rotenberg, Phys. Rev. B **60**, 17 030 (1999).
[16] A. P. Graham, D. Fang, E. M. McCash, and W. Allison, Phys. Rev. B **57**, 13 158 (1998).
[17] T. C. Q. Noakes, P. Bailey, and G. van der Laan, Phys. Rev. B **67**, 153401 (2003).
[18] S. Müller, B. Schulz, G. Kostka, M. Farle, K. Heinz, and K. Baberschke, Surf. Sci. **364**, 235 (1996).
[19] W. Platow, U. Bovensiepen, P. Poulopoulos, M. Farle, K. Baberschke, L. Hammer, S. Walter, S. Müller, and K. Heinz, Phys. Rev. B **59**, 12 641 (1999).
[20] D. Spišák and J. Hafner, J. Phys. Condens. Matter **12**, L139 (2000).
[21] K. Lenarčič-Poljanec, M. Hodošček, D. Lovrić, and B. Gumhalter, Surf. Sci. **251–252**, 706 (1991).
[22] A. Chizmeshya and E. Zaremba, Surf. Sci. **220**, 443 (1989).
[23] A. Chizmeshya and E. Zaremba, Surf. Sci. **268**, 432 (1992).
[24] C. Schwartz and R. J. Le Roy, Surf. Sci. **166**, L141 (1986).